IEEE Access
Multidisciplinary | Rapid Review | Open Access Journal

Received February 12, 2022, accepted February 28, 2022, date of publication March 8, 2022, date of current version March 16, 2022.

Digital Object Identifier 10.1109/ACCESS.2022.3157294

Optimal Operation Approach With Combined BESS Sizing and PV Generation in Microgrid

YONG-RAE LEE, HYUN-JOON KANG, AND MUN-KYEOM KIM
School of Energy System Engineering, Chung-Ang University, Dongjak-gu, Seoul 06974, Republic of Korea
Corresponding author: Mun-Kyeom Kim (mkim@cau.ac.kr)

This work was supported in part by the Basic Science Research Program through the National Research Foundation of Korea (NRF) by the Ministry of Education under Grant 2020R1A2C1004743, and in part by the Chung-Ang University Research Scholarship Grant 2021.

ABSTRACT Photovoltaic (PV) energy generation in microgrids (MGs) is increasing. Battery energy storage systems (BESSs) reduce the fluctuations in PV outputs caused by the intermittent availability of solar energy. Although BESSs are advantageous for stable MG operation, they are still relatively expensive. By remaining within the operational limits during normal and contingency operation, optimal sizing of BESS is required to maintain security considering cost of MG system. This paper proposes a BESS sizing optimization approach for MGs by solving the security constrained optimal power flow (SCOPF), considering the stochastic errors in forecasting the PV outputs. The degree of compensation for the solar energy forecasting error is firstly configured. To address these errors, the combined PV and BESS operation system is modeled by applying a control strategy to smooth PV fluctuations and minimize battery life degradation. BESS sizing optimization, under a certain degree of compensation, minimizes the PV penalty cost and BESS operation cost. The optimal BESS capacity and schedule are then obtained for the MG. To enhance the convergence and computational efficiency, decomposed-probabilistic security constrained optimal power flow (D-PSCOPF) is proposed. It efficiently solves the problem by dividing it into a master problem and a slave problem. The base case solution is computed in the slave problem, which induces the partial optimal size of BESS. By adding the feasibility cut through the violation of the slave problem, the master problem derives the optimal BESS capacity. Different case studies were analyzed, confirming the superiority and computational efficiency of the proposed approach.

INDEX TERMS Battery energy storage system, decomposed-probabilistic security constrained optimal power flow, PV forecasting errors, size optimization efficiency, smoothing control strategy.

NOMENCLATURE

A. INDICES AND SETS

t	Index over time periods.
T	Set of indices of time periods.
j	Index over scenarios.
J	Set of indices of all scenarios.
k	Index over post-contingency cases.
K	Set of indices of contingencies considered in scenarios.
i	Index over injections.
I^t	Set/maximum number of uncertainties available for dispatch in any contingency at time t.
n	Number of samples in a scheduling cycle.
c	Electricity price.

The associate editor coordinating the review of this manuscript and approving it for publication was S. Ali Arefifar.

B. PARAMETERS

g^{tjk}	Power flow equations in post contingency state k of scenario j at time t.
h^{tjk}	Transmission, voltage and other limits in post-contingency state k of scenario j at time t.
R^{ti}_{max+}, R^{ti}_{max-}	Upward/downward contingency reserve capacity limits for unit i at time t.
C^{ti}_{p}	Cost function for active injection i at time t.
$C^{ti}_{R_+}$, $C^{ti}_{R_-}$	Cost function for upward/downward contingency reserve from unit i at time t.
$C^{ti}_{\delta_+}$, $C^{ti}_{\delta_-}$	Cost of upward/downward load-following ramp reserve for unit i at time t.
C_{s0}	Vector of costs by storage unit associated with starting out.

C_v^{ti}	Startup costs for unit i at time t in \$ per startup.
C_w^{ti}	Shutdown costs for unit i at time t in \$ per shutdown.
C_{ts0}	Weighted price vectors summarizing
C_{tsc}	contributions to the value of terminal
C_{tsd}	storage.
γ^t	Probability of making it to period t without branch off the central path in a contingency in periods.
$P_{PV,actual}$	Actual power output of PV.
$P_{PV,forecast}$	Forecasted power output of PV.
P_{rate}	Required rated power of the BESS.
P_{BESS}	Actual charging and discharging power of the BESS.
E	Energy fluctuation of BESS at the sampling time relative to the initial state.
E_{rate}	Rated capacity of the BESS.
Q_{cycle}	Capacity loss at the time instants.
P_G	Combined output power of the system.
f_α	Confidence rate cost.
$f_{\alpha,penalty}$	Penalty cost of the PV operation at $\alpha\%$.
$f_{\alpha,BESS}$	cost of installation and life cycle of BESS at $\alpha\%$.
$f_{\alpha,curtail}$	Cost of the PV curtailment at $\alpha\%$.
$f_{\alpha,reserve}$	Cost of the reserve provision at $\alpha\%$.
$f_{\alpha,install}$	Installation cost of BESS at $\alpha\%$.
$f_{\alpha,LC}$	Life cycle cost of BESS at $\alpha\%$.
F	Probability distribution function of errors.
S_k	Objective function of Slave problem.
G	Equality constraints.
H	Inequality constraints.
S	Objective function of Master problem.

C. VARIABLES

p^{tijk}	Active injection for unit i in post-contingency state k of scenario j at time t.
P_+^{tijk}	Upward deviation from active power contract quantity for unit i in post-contingency state k of scenario j at time t.
P_-^{tijk}	Downward deviation from active power contract quantity for unit i in post-contingency state k of scenario j at time t.
r_+^{ti}	Upward active contingency reserve quantity provided by unit i at time t.
r_-^{ti}	Downward active contingency reserve quantity provided by unit i at time t.
δ_+^{ti}, δ_-^{ti}	Upward/downward load following ramping reserves needed from unit i at time t.
θ^{tjk}	Voltage angles for power flow in post-contingency state k of scenario j at time t.
V^{tjk}	Voltage magnitudes for power flow in post-contingency state k of scenario j at time t.
p^{tjk}	Active injections for power flow in post-contingency state k of scenario j at time t.
q^{tjk}	Reactive injections for power flow in post-contingency state k of scenario j at time t.
p_{sc}, p_{sd}	Charge/discharge power injections of storage unit.
v^{ti}, w^{ti}	Binary startup/shutdown states for unit i in period t.
e	Error of PV power forecast.
α	Confidence rate.
$e_{\alpha low}$, $e_{\alpha high}$	Lower/higher bound of the confidence level at $\alpha\%$.
Δt	Sampling period.
SOC_{up}, SOC_{low}	Upper/lower limit constraints of the SOC.
γ, β	Fitting coefficients.
E_α	Activation energy.
R_{gas}	Gas constant.
T_K	Ambient temperature.
Ah	Ampere-hour throughput.
z	Power-law factor.
$V_{nominal}$	Nominal voltage.
$\phi(\delta_g)$	Cycle depth of BESS.
R	Battery-cell replacement cost.
η	Charging/discharging efficiency.
C_{BESS}	Battery current for charge.
$E_{curtail}$	Capacity of PV curtailment.
$E_{reserve}$	Capacity of reserve provision.
X	State variables.
U	Control variables.

D. ABBREVIATIONS

PV	Photovoltaic.
MG	Microgrid.
BESS	Battery energy storage system.
SCOPF	Security constrained optimal power flow.
D-PSCOPF	Decomposed probabilistic security constrained optimal power flow.
RES	Renewable energy source.
SOC	State of charge.
DOD	Depth of discharge.

I. INTRODUCTION

A. BACKGROUND

Microgrids (MGs) have received increasing attention as a means of integrating distributed generation into the power system [1]. MGs are usually described as confined clusters of loads, energy storage systems (ESSs), renewable energy sources (RESs), and traditional generators. A fundamental tool in power grid analysis is the optimal power flow (OPF) [2]. OPF aims to minimize operational cost while ensuring secure operation within the technical limits of the power system. In current operational schemes, a system is considered secure when it remains within the operational limits on normal operation as well as contingency situations.

This principle is reflected in the OPF through additional constraints, to a security constrained optimal power flow (SCOPF) [3].

Forecast uncertainty in MGs is a disturbance affecting the system. Forecast uncertainty arises from unpredictable fluctuations in the RESs. With increasing RES penetration rate, it has become necessary to explicitly account for uncertainty while solving the optimization problems. Probabilistic security constrained optimal power flow (PSCOPF) has been utilized in the MGs as a solution to the security problem, which has become more critical due to RES uncertainties [4]. One of the RESs, photovoltaic (PV) generation, has developed rapidly in recent years and is mostly used in inland MGs. To avoid the adverse effects of PVs on MGs, additional equipment resources and a methodological technique, such as uncertainty modeling or probabilistic optimization methods, are required. The battery energy storage system (BESS) is a flexible regulated device developed to solve these problems by smoothing the short-term PV output fluctuations. The operation and size of BESS are key factors affecting the smoothing effects. However, due to the relatively high cost of the BESS, optimization of the BESS sizing is indispensable. Accordingly, it is necessary to use PSCOPF to determine the optimal sizing of BESS to ensure economical operation as well as security in the MG.

B. LITERATRUE REVIEW

Solar energy photovoltaics (PVs) are one of the most abundant RESs. They are expected to be a clean power electricity source in meeting electricity demands. Further, they have broad applications in industrial, domestic, and generation systems. However, connecting a significant number of PVs to the grids of power utilities in the future could cause problems in power system operations due to power output fluctuations [5]–[7]. The problem of smoothing out power fluctuations in PV generation has attracted interest in MG-related research. Many measures have been incorporated in PV system design to meet the demands of a large PV penetration in the system. Specifically, several control strategies and configurations for hybrid energy storage devices, such as BESS [8]–[10], superconducting magnetic energy system [11], a flywheel energy system [12], an energy capacitor system [13], [14], and a fuel cell hybrid system [15], have been proposed to smooth solar power fluctuations or enhance power quality.

Different batteries that have distinctive characteristics, such as energy storage density, charge/discharge rate, life cycle, and cost. BESSs can provide flexible energy management solutions to control PV power fluctuations, thus improving the power quality of renewable energy generation systems.

Conventional control strategies for mitigating PV output fluctuations using BESS typically determine the amplitude of the power fluctuations and then adjust the BESS output [16]. In [17], BESS is used to optimize the distribution networks that include PV, and the influences of BESS parameter are analyzed from PV uncertainty. Least squares minimization technique is used in [18] to minimize the error between the targeted smoothed power and the smoothed reference curves. When the PV power exceeds limits, the BESS is charged or discharged to meet the requirements. However, this strategy may not be feasible during intervals when the state of charge (SOC) limit is exceeded. Because the BESS is expensive, the BESS capacity needs to be optimized [19]. With the advances in power generation, extensive of research on BESS sizing has been conducted. An analytic approach of sizing BESS is developed in [20] providing a simple and flexible economic analysis to estimate the profitability of ESS to address the ESS sizing problem. In [21], optimal sizing of renewable energy sources and BESS are conducted considering the non-controllable parameters impacting the renewable energy output. In [22], the size of the BESS on a university campus was optimally determined using predictions of load and PV generation. A BESS sizing method for a grid-connected PV generator application was proposed in [23], which considered the technical requirement and economic benefits of power systems. An optimization model for sizing the BESS of grid-connected PV systems was presented in [24]; the objective of this work is to minimize the net power purchase cost from the electric grid and the BESS capacity loss with an electricity price change. In [25], a performance-based sizing method involved using BESS at a house, distribution transformer, and community levels with a high PV penetration. In [26], a flywheel ESS considering conventional generators was sized using the genetic algorithm.

SCOPF is a useful tool for ensuring safe operation of power systems when renewable generators, such as wind turbine generators, which introduce uncertainty, are connected to the system [27]. It considers some contingencies, such as generators and line outages. SCOPF ensures minimum cost, safe operation, and system security by evaluating the impact of renewables on power systems' security of priority caused by the intrinsic uncertainties of RESs [28]. Ref. [29] not only considered a power system with high renewable source penetration, but also developed a security constrained model to assess the impact of BESS units on the security of the system. To secure the system against the uncertainties of renewable generations, the required capacity of BESS was increased. The increasing BESS capacity necessitated charging/discharging cycle and size optimization involving complex calculations. In [30]–[32], the BESS operation under increased capacity was simplified. However, to significantly reduce, the convergence and computational speed, an idealized BESS was operated without considering cycle aging and several other constraints. Consequently, the calculated operating cost and optimal capacity was unrealistic. However, it is possible to obtain a computational efficiency that reflects actual BESS operation by decomposing the complex problem while considering the operation and sizing of the BESS, which maintains the stability of the system despite the increase of RESs.

C. CONTRIBUTIONS AND PAPER ORGANIZATIONS

This study presents a novel BESS sizing optimization approach by addressing the decomposed PSCOPF (D-PSCOPF) problem of an isolated MG with PV generators. Here, the BESS is operated to counter PV fluctuations and prediction errors to maintain the stability of the system. The proposed approach not only solves the stability problem caused by introducing PV by obtaining the optimal BESS capacity, but also brings economic benefits by minimizing the cost of the BESS and the penalty cost of the PV. The main contributions of this study can be summarized as follows

- By approaching the PV forecasting error as an index of confidence rate, even though various PV prediction techniques exist, the interval of error that can compromise economic and stability can be determined through historical PV forecasting and actual data.
- PV fluctuation smoothing strategy based on dynamic SOC regulation is proposed. The accuracy of combined PV-BESS operation system is increased through the BESS compensation strategy considering the rated output/capacity and life degradation model of the BESS in our strategy.
- Using BESS sizing optimization with PV generation, the partial optimal BESS capacity can be obtained for the predefined confidence rate that minimizes the initial installation cost, aging cost, and penalty cost of PV according to the capacity of the BESS.
- To reduce the computational burden and improve the convergence, the proposed D-PSCOPF problem is solved through Benders decomposition (BD). In BD, the master problem solves PSCOPF without considering the PV/BESS operation. The slave problem finds the optimal BESS capacity that does not affect the stability of the system. If a security constraint is violated, a feasibility cut is added to the master problem and the BESS sizing is obtained again.

The remainder of this paper is organized as follows. Section II details the PSCOPF modeling and analysis. Section III addresses BESS compensation strategy, including combined PV-BESS operation system. Section IV models BESS sizing optimization approach. Section V proposed D-PSCOPF modeling which applied decomposition method. Section VI provides the simulation results for different case studies, and Section VII concludes the paper.

II. OPTIMIZATION MODELING

A. PSCOPF MODEL

The optimization model used in this study is a PSCOPF model that is improved to study the impact of the RESs and BESSs. The characteristics of PSCOPF can be summarized as follows. It allows deterministic information to be processed as input, as well as stochastic information, which represents a probability distribution. Thus, it can analyze variable renewable generation that has a stochastic nature due to its inherent variability, and it can be used in the optimal BESS operational planning as well as its impact on the MG. Moreover, this model calculates the required reserves to maintain the power system security, which is an indispensable component for the reliable operation of the MG. Therefore, PSCOPF is advantageous for computing the cost of PV generation uncertainty because different types of reserves can be determined to address the variability of renewable generation.

1) OBJECTIVE FUNCTION

The objective function aims to minimize the cost function of MG operation, and it consists of six cost functions.

$$\min_{x} f(x) \tag{1}$$

where

$$f(x) = f_p(p, p+, p-) + f_r(r+, r-) + f_\delta(p) + f_I(\delta+, \delta-) + f_s(s_0, p_{sc}, p_{sd}) + f_g(v, w) \tag{2}$$

Equations (1)–(2) show a reduced form of the objective function of PSCOPF, which is structured to minimize expected operating costs with respect to reserve costs, by considering the stochastic RESs. The cost for active power dispatch and redispatch are related to the amount of generated power and the deviation between contracted power in day-ahead t and real-time markets.

$$f_p(p, p+, p-) = \sum_{t\in T}\sum_{j\in J}\sum_{k\in K}\phi_\alpha^{tjk} \times \sum_{i\in I}[C_p^{ti}\left(p^{tijk}\right) + C_p^{ti} + P_+^{tijk} + C_p^{yi} - p_i^{tijk}] \tag{3}$$

Equation (3) represents the cost related to the operation cost of the generator, with the output being computed per generator.

The contingency reserve cost is related to balancing the net load uncertainty within an hour.

$$f_r(r+, r-) = \sum_{t\in T}\gamma^t\sum_{i\in I}[C_{R_+}^{ti}\left(r_+^{ti}\right) + C_{R_-}^{ti}\left(r_-^{ti}\right)] \tag{4}$$

Equation (4) is used to determine unexpected accident events such as generator failure or transmission line failure.

Load-following ramp reserve cost are incurred when meeting hour-to-hour variability of net load.

$$f_\delta(p) = \sum_{t\in T}\gamma^t\sum_{j\in J}\phi^{tj}\sum_{i\in I}C_\delta^i(p^{tij} - p^{(t-1)ij}) \tag{5}$$

Equation (5) shows the penalty cost of PV generation, which can cause severe output changes according to the high variability of the PV output. Load-following ramping cost is related to life degradation due to the stress on conventional generators. Typically, it is attributed to high variability in renewable generation.

$$f_I(\delta+, \delta-) = \sum_{t\in T}\gamma^t\sum_{i\in I}[C_{\delta_+}^{ti}\left(\delta_+^{ti}\right) + C_{\delta_-}^{ti}\left(\delta_-^{ti}\right)] \tag{6}$$

Equation (6) shows the cost of the load after required in case of a sudden change in power system load.

$$f_s\left(s_0, p_{sc}, p_{sd}\right) = C_{s0}s_0 - \left(C_{ts0}s_0 + C_{tsc}p_{sc} + C_{tsd}p_{sd}\right) \quad (7)$$

Equation (7) represents the cost related to settlement for the initial energy stored in the BESS and the residual energy from the last period.

Furthermore, starting up and shutting down conventional generators involves costs that affect unit commitment decisions, which are presented in (8).

$$f_g\left(v, w\right) = \sum_{t\in T}\gamma^t \sum_{i\in I}\left[\left(C_v^{ti}v^{ti} + C_w^{ti}w^{ti}\right)\right] \quad (8)$$

2) CONSTRAINTS

The above objective function must satisfy all constraints: basic OPF model constraints, contingency constraints, time variability control constraints, and generator operation schedule constraints.

$$g^{tjk}\left(\theta^{tjk}, V^{tjk}, p^{tjk}, q^{tjk}\right) = 0 \quad (9)$$

$$h^{tjk}\left(\theta^{tjk}, V^{tjk}, p^{tjk}, q^{tjk}\right) \le 0 \quad (10)$$

Equations (9) and (10) represent the nonlinear power balance equation, nonlinear grid constraint, voltage constraint, and other inequality constraints.

$$0 \le p_+^{tjk} \le r_+^{ti} \le R_{max+}^{ti} \quad (11)$$

$$0 \le p_-^{tjk} \le r_-^{ti} \le R_{max-}^{ti} \quad (12)$$

$$p^{tijk} - p_c^{ti} = p_+^{tijk} - p_-^{tijk} \quad (13)$$

Equations (11)–(13) represent the constraints related to the reserve capacity, redispatch, and contract variable.

III. BESS COMPENSATION STRATEGY

A. COMBINED PV AND BESS OPERATION SYSTEM

Configuring an appropriate BESS in the PV can allow for flexible control of the power grid. The BESS can decrease the uncertainty caused by the PV forecast error, thus meeting the goal of tracking the planned output. The BESS sizing optimization method proposed in this study is based on PV forecasting error, which attributable to the difference between the predicted and actual outputs of PVs. The rated power and capacity of the BESS depend on the PV forecasting error. The error of PV forecast (e) is formulated as

$$e = P_{PV,actual} - P_{PV,forecast} \quad (14)$$

By analyzing the PV historical data, the distribution of the forecasting error can be found, and the confidence intervals of errors under different confidence rates can then be obtained. Figure 1 shows the probability of occurrence due to the forecasting error value (p.u.). Our work assumes that the error obeys the commonly used normal distribution. The higher and lower bound of the confidence intervals are written as $e_{\alpha low}$ and $e_{\alpha high}$. A confidence rate of $\alpha\%$ implies that the probability of forecast error falls into the confidence interval $\alpha\%$.

B. BESS OPERATION FOR PV FORECASTING ERROR

1) RATED POWER OF BESS

The BESS is used to compensate for forecast error of the PVs when tracking the planned output of the PVs. Accordingly, the actual output of PVs follows the planned output (forecast). When the error is bigger than 0, that is, if the actual PV output is greater than the forecast output, the BESS charges, and the PVs avoid the penalty of PV curtailment. In contrast, when the error is smaller than 0, that is, if the actual PV output is less than the forecast output, the BESS discharges, which avoids the penalty of power shortage caused by a lack of power in the PVs. Installing appropriate BESS at the outlet of the PVs ensures that the PV output is as close to the planned output as possible.

The probability of a large PV forecast error is small when only considered statistically. To compensate for a large error with a small likelihood of occurrence, as shown in Fig. 1, it would be necessary to install a BESS with a high power rating. However, this increases costs. Therefore, the concept of error compensation rate is be considered in choosing an optimal BESS capacity. The error compensation rate $\alpha\%$ is defined as the BESS compensating $\alpha\%$ of the PV forecasting error. When the BESS compensates for all forecast errors, the error compensation rate is 100%, and the rated power of the BESS is the maximum absolute value of the forecast error.

$$P_{rate} = max\left|e\right| \quad (15)$$

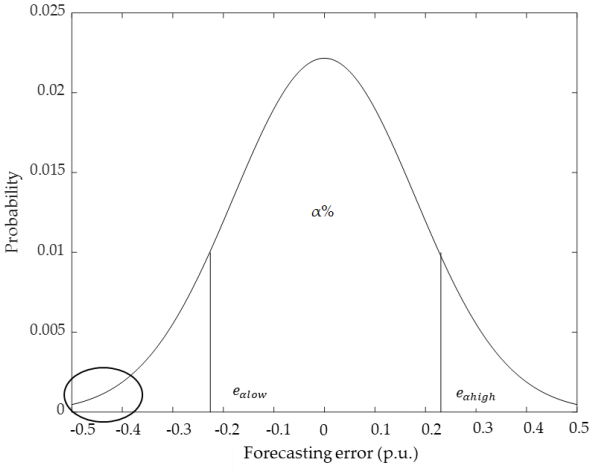

FIGURE 1. Probability density function of forecasting error.

The error compensation rate is $\alpha\%$ when the BESS compensates $\alpha\%$ error. Meanwhile, the error compensation is $(e_{\alpha low}, e_{\alpha high})$.

The required BESS rated power is maximum absolute value of the higher and lower bounds of the confidence interval as follows:

$$P_{rate} = max\left(\left|e_{\alpha low}\right|, \left|e_{\alpha high}\right|\right) \quad (16)$$

2) RATED CAPACITY OF BESS

Due to the different dispatching and operation plans of MG, the optimal BESS rated capacity can vary. In this work, one day is required to configure the BESS rated capacity. By accumulating the BESS charging and discharging at each sampling time, the energy fluctuation of BESS relative to the initial state at different sampling times can defined as

$$E(n) = \sum_{i}^{n} (P_{BESS}(i) \times \Delta t) \tag{17}$$

$$P_{BESS}(i) = \begin{cases} e, & e_{\alpha low} < e < e_{\alpha high} \\ e_{\alpha high}, & e > e_{\alpha high} \\ e_{\alpha low}, & e < e_{\alpha low} \end{cases} \tag{18}$$

The operation power of BESS is determined according to the higher and lower bound of confidence interval.

The difference between the maximum and minimum energy fluctuation during BESS operation can be calculated by considering the energy fluctuation during the whole sample data period. Considering the SOC limits, the required BESS capacity can be obtained, which is the rated capacity of the BESS.

$$E_{rate} = \frac{max(E(n)) - min(E(n))}{SOC_{up} - SOC_{low}} \tag{19}$$

In practice, the values should be appropriately selected in integer 0 or 1 to avoid over-charging and over-discharging during the actual operation of the BESS. When the compensation rate is 100%, the BESS can completely compensate for the PV forecasting error; $P_{BESS}(i)$ denotes the forecast error e of each sampling time. A compensation degree of $\alpha\%$, implies that the BESS compensated for a $\alpha\%$ error.

3) BATTERY LIFE DEGRADATION MODELING

Because of the battery's characteristics in electrochemical dynamics and physics, it is difficult to check the internal states accurately. Although there is a conflict between energy consumption and battery life extension, there have been various studies to minimize both energy consumption and battery degradation in terms of energy management [33]. Therefore, it is necessary to establish a control strategy to optimize power management and battery aging without loss of performance. To estimate the impact of battery degradation due to charging from PV generation, the cycle aging model is defined following [34]

$$Q_{cycle} = (\gamma SOC + \beta) \cdot \left(\frac{-E_\alpha + \eta \cdot C_{rate}}{R_{gas} \cdot T_K} \right) Ah^2 \tag{20}$$

Fitting coefficients γ and β are defined by the SOC dependence.

For investigating the charging cycles of the BESS during test time periods, a discrete model of cycle aging can be determined as follows:

$$Q_{cycle,n+1} - Q_{cycle,n} = \Delta Ah \cdot z(\gamma SOC + \beta) \cdot \left(\frac{-E_\alpha + \eta \cdot C_{rate}}{R_{gas} \cdot T_K} \right) Ah_n^{z-1} \tag{21}$$

In this study, throughput in amp-hours is defined as energy divided by nominal voltage as

$$\Delta Ah = \frac{1}{3600} \int_{t_m}^{t_{n-1}} |C_{BESS}(t)| \, dt \approx \frac{E}{V_{nominal}} \tag{22}$$

$$Ah_{n+1} = Ah_n + \Delta Ah \tag{23}$$

the most important characteristics are the SOC and SOC swing that affect the state of the degradation of the battery. The SOC of BESS represents the ratio of the charged capacity. Meanwhile, the SOC swing is defined as the change in the SOC level during a cycle of charging and discharging. Fig. 2 depicts the relationship between SOC and SOC swing with the number of available cycles for the lifetime of BESS, which is based on the experimental results. Based on these BESS degradation characteristics, BESS operation with a lower average SOC and swing results in a higher expected cycle life. This allows the most efficient BESS operation strategy to be established in the MG system.

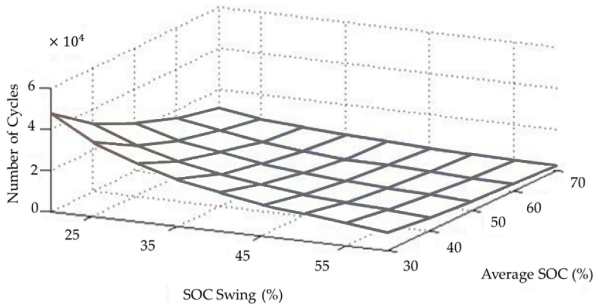

FIGURE 2. Number of life cycles according to SOC characteristics.

4) PV FLUCTUATION SMOOTHING CONTROL STRATEGY

The traditional control strategy to smooth the PV output fluctuation in the BESS typically determines the amplitude of the power fluctuation, and then provides an instruction to the BESS. In this strategy, if the PV power exceeds the threshold, the BESS charges or discharges to meet the requirements. However, when the SOC reaches its threshold, the BESS is unable to execute the instructions. Therefore, our study suggests several approaches to simultaneously solve these problems. The first approach is to increase the size of the BESS. This improves the PV fluctuation, but also increases the cost. The second approach is to design a more effective control strategy to improve the smoothing ability. The first part is a real-time control strategy for smoothing the PV fluctuation. It is designed to determine whether the PV fluctuation exceeds the threshold, and charging or discharging is required to maintain the power fluctuation in a predefined adequate

boundary as follows:

$$P_{BESS}(t) = \begin{cases} P_{PV}(t) - P_G(t-1) - P_{max}, \\ \quad P_{PV}(t) - P_G(t-1) > P_{max} \\ P_{PV}(t) - P_G(t-1) + P_{max}, \\ \quad P_{PV}(t) - P_G(t-1) < -P_{max} \end{cases} \tag{24}$$

The second part is an SOC-regulated strategy based on short-term prediction and is designed to determine whether the SOC of the BESS exceeds the normal boundary. The SOC is dynamically regulated when the PV fluctuation does not exceed the normal boundary. If the SOC exceeds the normal boundary, the BESS charges or discharges to recover the SOC to a more appropriate range. For calculating the regulated power of the BESS more rationally, a dynamic SOC regulation-based PV output prediction is considered.

To facilitate our strategy, two state variables S1 and S2 are defined. S1 represents the state value that indicates whether the BESS is required to charge or discharge as the first action. S2 represents the state value that indicates whether or not the BESS acts during the entire period. S1 = 1 implies that the first action of the BESS is discharging, whereas S1 = 0 indicates that the first action of the BESS is charging. In contrast, S2 = 1 implies that the BESS does not act during the entire period, whereas S2 = 0 implies that the BESS acts during the entire period. The charging and discharging of the BESS are formulated as follows:

$$(t) = \begin{cases} min\left(\begin{array}{l} P_{max} - |P_{PV}(t) - P_G(t-1)|, \\ (SOC(t) - SOC_{high}) \times \dfrac{E_{rate}}{\Delta t} \end{array}\right), \\ SOC(t) > SOC_{high}, \quad S1 = 1 or S2 = 1 \\ min\left(\begin{array}{l} P_{max} - |P_{PV}(t) - P_G(t-1)|, \\ (SOC(t) - SOC_{low}) \times \dfrac{E_{rate}}{\Delta t} \end{array}\right), \\ SOC(t) < SOC_{low}, \quad S1 = 0 \; or \; S2 = 1 \\ 0, \quad others \end{cases} \tag{25}$$

When the SOC is greater than SOC_{high}, the BESS charges first (S1 = 1) or does not act (S2 = 1) in the predicted period, and the BESS must discharge to obtain more capacity to charge soon. When the SOC is lesser than SOC_{low}, the BESS discharges first (S1 = 1) or does not act (S2 = 1) in the predicted period, and the BESS charges.

IV. BESS SIZING OPTIMIZATION APPROACH

To optimize the BESS sizing under a certain compensation degree, the compensation interval of the forecasting error from this compensation degree must be first obtained in the combined PV-BESS. The error compensation interval is not unique under the same compensation degree. Our study aims to determine the optimal interval, and then obtain the optimal BESS sizing to minimize the cost of installation of the PV-BESS. As shown in figure 3., optimal BESS sizing starts with input historical PV, load, and generator data. From the derived data of predicted and actual PV outputs, confidence rate $\alpha\%$ and confidence interval [$e_{\alpha low}$, $e_{\alpha high}$] are obtained.

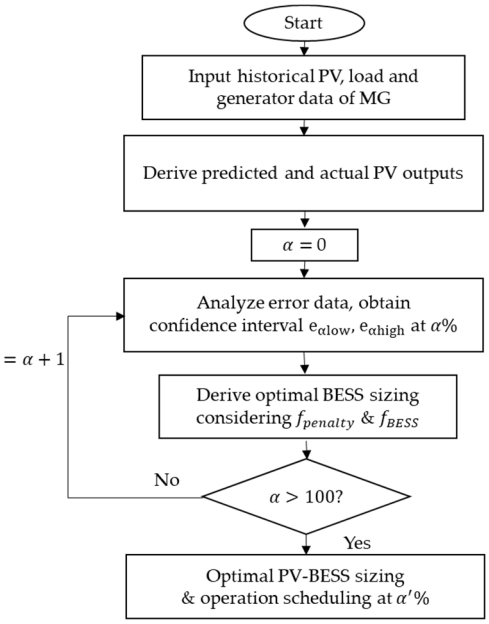

FIGURE 3. Optimal BESS sizing process.

By considering $f_{penalty}$ and f_{BESS} at $\alpha\%$, optimal BESS capacity is obtained from following subsection. α begins at 0% and repeats up to 100%. After comparing all the results, the lowest cost is found at $\alpha'\%$, and the BESS capacity at $\alpha'\%$ is determined as the optimal capacity.

5) OBJECTIVE FUNCTION

Considering the economic index of PV-BESS, the objective function is to minimize the confidence rate cost (f_α), which is consisted of penalty cost of the PV and the operation cost of BESS at a confidence rate $\alpha\%$.

$$min\, f_\alpha = f_{\alpha,penalty} + f_{\alpha,BESS} \tag{26}$$

where f_α is the objective function, and it is divided into the penalty cost of the PV and operation cost of the BESS.

$$f_{\alpha,penalty} = f_{\alpha,curtail} + f_{\alpha,reserve} \tag{27}$$

$$f_{\alpha,BESS} = f_{\alpha,install} + f_{\alpha,LC} \tag{28}$$

$$f_{\alpha,penalty} = c_1 \times E_{curtail} + c_2 \times E_{reserve} \tag{29}$$

where c_1 and c_2 denote the unit PV curtailment cost and the unit cost of the reserve provision, respectively.

$$E_{curtail} = \sum_i^n \lambda \times \left(e[i] - e_{\alpha high}\right) \times \Delta t$$
$$\lambda \begin{cases} 0, & e[i]] < e \\ 1, & e[i]] \geq e_{\alpha high} \end{cases} \tag{30}$$

$$E_{reserve} = \sum_i^n \lambda \times (e[i] - e_{\alpha low}) \times \Delta t$$
$$\lambda \begin{cases} 0, & e[i]] > e_{\alpha low} \\ 1, & e[i]] \leq e_{\alpha high} \end{cases} \tag{31}$$

Here, the $E_{curtail}$ and $E_{reserve}$ are determined according to the confidence interval ($e_{\alpha low}$, $e_{\alpha high}$).

$$f_{\alpha,BESS} = c_{install} \times E_{rate} + \frac{R}{\eta E_{rate}} \phi(\delta_g) \tag{32}$$

In equation (32), the second form represents the life cycle cost of the BESS.

6) CONSTRAINTS

Constraints on the rated power of the BESS are determined as

$$0 \le P_{rate} \le max\,|e| \tag{33}$$

$$F\left(e_{\alpha high}\right) - F\left(e_{\alpha low}\right) = \alpha\% \tag{34}$$

Equation (33) represents the constraint on the rated power of the BESS, and (34) represents the constraint on the higher and lower bounds of the error confidence intervals.

V. PROPOSED D-PSCOPF MODEL

In the previous section, the optimal BESS capacity was calculated according to the confidence interval of the PV volatility. However, this value represents the partial optimal BESS capacity only in the confidence interval derived from the specific confidence level α. This partial optimal BESS capacity is added as a BESS constraint to the SCOPF problem, and the PV penalty cost is then derived by charging/discharging the BESS caused by this BESS capacity. This PV cost is considered to the partial optimization of the BESS capacity and varies the capacity calculation. In this way, it is complicated to solve the problem that the result variable (PV penalty cost) affects the cause variable (partial optimal BESS capacity). Benders decomposition [35] is used to facilitate such a complex calculation where the solution is based on decomposing the problem into master and slave problems. Information from the slave problem is used to determine whether the solutions of the master problem and the slave problem variable values are optimal. When a violation is detected in the slave problems, Benders cut is created. This restores corresponding constraints back to the master problem. As this process is repeated, Benders decomposition guarantees that it converges to the optimal solution. D-PSCOPF is applied to PSCOPF based on the method of Benders decomposition. Through D-PSCOPF, this problem can be efficiently solved by dividing it into a master problem and slave problem, either. First, in the slave problem of determining the partial optimal BESS capacity, the base case solution is calculated. Using this value, the PV penalty cost is obtained from the master problem, and this cost is again included in the constraints of the slave problem, which includes the sizing process of the BESS. At this time, when a violation occurs, a feasibility cut is added to the main problem. As the feasibility cut is repeatedly created, the master problem and the slave problem converge to the optimal value which is derived at the point where the cut is not created. Thus, the results of the master problem and the slave problem converge to the same optimal solution. When the BESS compensates the error of α, we refer to the error compensation rate as α. Currently, the error compensation is ($e_{\alpha low}$, $e_{\alpha high}$), where $e_{\alpha low}$ and $e_{\alpha high}$ denote the lower and upper bounds of the compensation interval, respectively.

A. SLAVE PROBLEM

The objective of the slave problem is to minimize the operating cost of the PV-BESS and is formulated in (26)– (34). The objective function is composed as follows:

$$\begin{aligned} S_k\,(u_o) = Min\, & f_{\alpha,penalty} + f_{\alpha,BESS} \\ s.t.\ & G_\alpha\,(X_\alpha, U_\alpha) = 0, \\ & H_\alpha^{min} \le H_\alpha\,(X_\alpha, U_\alpha) \le H_\alpha^{max}, \\ & \delta_\alpha \le \delta_{\alpha'}, \quad \alpha = 1, 2, \ldots, 100 \end{aligned} \tag{35}$$

The last equation is not included in objective function of BESS sizing operation with PV generation, but it is a constraint of the depth of discharge (DOD) of BESS that affects $f(\alpha,\ LC)$. If the objective function is equal to 0, the feasible solution u_i is obtained from the i-th slave problem. Conversely, if the objective function is greater than zero, the slave problem supplies constraints including violations to the master problem.

B. MASTER PROBLEM

The master problem is formulated as (1)–(13), and the constraints are updated by Benders cuts. In the master problem, the optimization problem is expressed as follows:

$$\begin{aligned} Min\ S\,(U_0) = & f_p\,(p, p+, p-) + f_r\,(r+, r-) \\ & + f_\delta\,(p) + f_I\,(\delta+, \delta-) \\ & + f_s\,(s_0, p_{sc}, p_{sd}) + f_g(v, w) \\ st.\ & G\,(X_0, U_0) = 0 \\ & H_{min} \le H\,(X_0, U_0) \le H_{max} \\ & S_k\,(u_0) \le 0 \end{aligned} \tag{36}$$

The last constraint defined in (37) is referred to as a feasibility cut. This is a linear constraint that limits the feasible area to adjust the coordination of the solutions of the master problem and subproblems. The feasibility cut is generated by the ramp reserve constraint from the slave problem, which is applied to the master problem when there is insufficient BESS capacity. After receiving an updated BESS capacity and PV schedule, the master problem repeats the iteration process by providing the PV penalty cost to the slave problem. $S_k(u_0) = 0$ represents the feasible cost result of the scenarios, whereas $S_k(u_0) > 0$ implies that the scenario result is not feasible.

C. SOLUTION PROCEDURE

Figure 4 depicts the optimization process of calculating the optimal BESS capacity through D-PSCOPF. The overall procedure can be implemented sequentially.

Step 1: Model the MG with generators and load.

Step 2: Set the capacity of PV to be added in MG, and obtain PV forecast based on historical PV generation data.

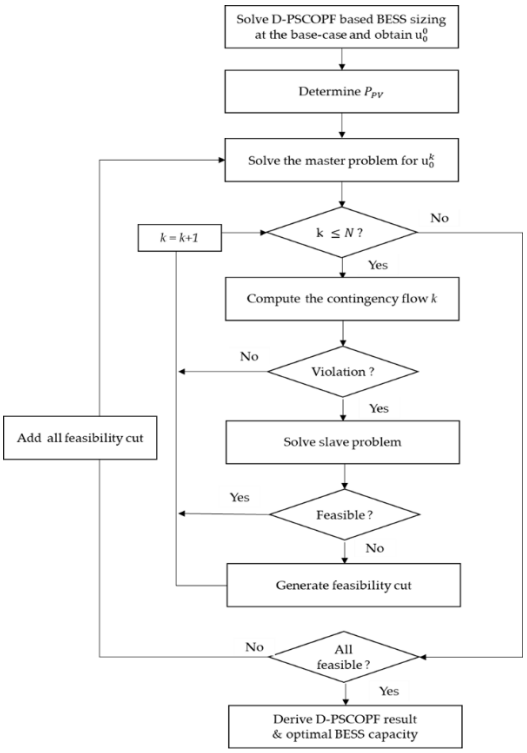

FIGURE 4. Procedure of D-PSCOPF model.

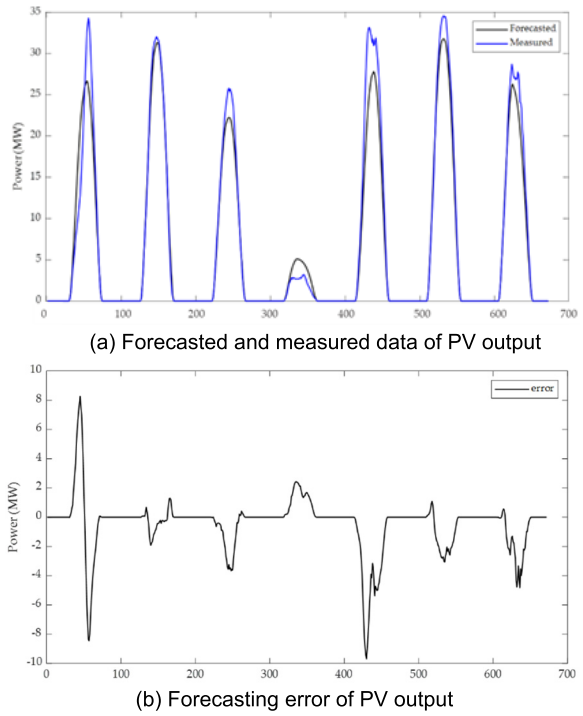

FIGURE 5. Output and error data of PV for a week in Brussel.

Step 3: Set the initial confidence degree α.
Step 4: Derive BESS scheduling according to α.
Step 5: Calculate the optimal BESS sizing through D-PSCOPF considering BESS capacity.
Step 6: Using the D-PSCOPF result, the cost of BESS and system stability are expressed as cost.
Step 7: Return to Step 3, iterate Step 3∼6 applying different confidence degrees.
Step 8: Determine the most suitable confidence rate, derive the optimal BESS size and D-PSCOPF results in that case.

VI. CASE STUDY

The proposed D-PSCOPF has been implemented on a 6-bus system [36] and a 14-bus system [37]. In our study, one of the main purposes of the BESS is to maintain the PV output following the forecasted data based on our BESS compensation strategy. Fig. 5 depicts PV data from Brussels, Belgium [38]. As shown in Fig. 5(a), field data of PV generators from 1 March to 7 March 2021 were applied in this work. The sampling interval was 5 min, time window was one day, and maximum output of the PV generators was 54.59 MW. Brussels' actual PV data was scaled by the penetration rate to use the error of the current prediction technique. Fig. 5(b) depicts the error of the measured PV power output in which approximately 30% of the maximum error exists. The D-PSCOPF was implemented using the Matlab software.

To demonstrate the superiority of our BESS sizing optimization approach, several cases of different approaches were evaluated. In Case 1, the BESS capacity was set to a fixed value according to the PV capacity. Thus, the maximum value of PV error is preset, and the BESS capacity was already determined according to the PV error. In Case 2, BESS sizing was performed according to the confidence interval, without the consideration of security constraints. Finally, Case 3 was optimized using the proposed approach.

A. 6-BUS SYSTEM

As shown in Fig. 6, the 6-bus system contains 11 transmission lines and 3 power generation units. Three PV generators and three BESSs are located in buses 1, 5, and 6. The total load is 199.5 MW, which is equally distributed among the three

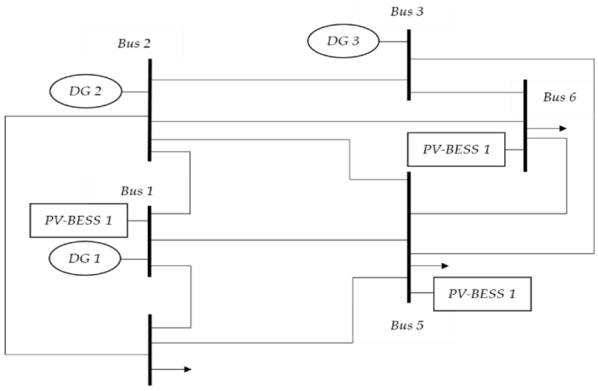

FIGURE 6. 6-bus test system.

loads. The characteristics of the DGs and PV generator are listed in Table 1.

TABLE 1. Technical data of generating units.

Source	Cost Coefficient ($/MWh)	P_{min} (MW)	P_{max} (MW)	RU (MW/h)	RD (MW/h)	Min U/D Time (h)
DG 1	27.7	20	100	50	50	3
DG 2	39.1	20	100	50	50	3
DG 3	61.3	16	60	60	60	1
DG 4	65.6	16	60	60	60	1
PV	0	0	30	-	-	-

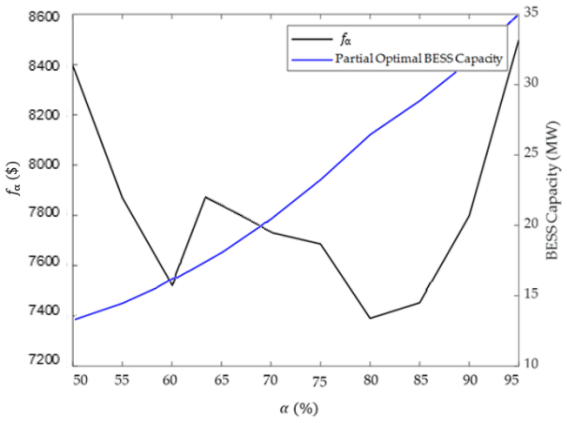

FIGURE 7. Partial optimal BESS capacity according to f_α.

Fig. 7 depicts the BESS capacity for each reliability and the confidence rate cost (f_α) according to the confidence rate. The BESS capacity decreases as the confidence interval increases, even though f_α exhibits a local minimum cost at 60% and a minimum cost at 80%. The partially optimal BESS capacity is determined according to the confidence degree of the error, and penalty cost ($f_{penalty}$) and BESS cost (f_{BESS}) are then determined from the BESS capacity. At this time, the partially optimal BESS capacity in consideration of these costs is obtained. The D-PSCOPF optimization is performed according to this capacity and an overall cost result is determined. If security is violated in the process of inserting the BESS capacity into D-PSCOPF, the BESS capacity is modified through BD, and the optimal size and cost of the BESS capacity are derived as a result.

Fig. 8 depicts the cost and SOC of each case. Here, the solid line indicates the PV penalty cost, dashed line represents the BESS cost, and dotted line indicates the SOC of the BESS. In all cases, penalty costs remain at $0 while the PV power is not generated, but they start to increase as the PV generators run. Case 1, with a fixed BESS capacity (highest capacity) without consideration of the PV prediction error, shows that the penalty cost curve of the PV is the lowest in all time periods, but the BESS cost and SOC curves are the highest among all cases. Case 2 demonstrates the highest penalty cost, but also yields a significantly lower BESS cost compared to that in Case 1. It can be observed from Fig. 8 that the SOC curve is also lower than that in Case 1. The penalty cost curve in Case 3 is higher than that in Case 1 and lower than that in Case 2 in all time windows. In addition, the cost curve of the BESS is higher than that in Case 2 and lower than that in Case 1. Because the sum of each cost is minimized by the BESS sizing optimization according to PV, the cost curves of Case 3 exist between those of Cases 1 and 2.

TABLE 2. Optimal results for each case.

Case	Penalty Cost ($)	BESS Cost ($)	Generation Cost ($)	Total Cost ($)	BESS Capacity (MW)
1	2,726	7,184	844,542	854,452	60
2	3,511	5,760	835,784	845,055	56
3	3,027	6,050	819,875	828,952	53.2

Table 2 shows the optimal results for the three cases. As a result of focusing on minimizing PV volatility in Case 1, the penalty cost is the lowest at $2,726. Meanwhile, the BESS cost is $7,184, indicating the highest cost among the three cases. Thus, it has the highest value in terms of power generation cost and overall cost despite minimizing the penalty cost. The optimal BESS capacity at this time is 60MW. In Case 2, which proceeded with BESS sizing without considering security constrained, the cost of BESS is the lowest at $5,760, but the penalty cost is about $800 higher than that of Case 1. The overall cost is reduced by about $9,400 compared to Case 1. In Case 3, the sum of the penalty cost and the BESS cost was the lowest among all cases. Also, the power generation cost and overall cost show the lowest results, and the capacity of the BESS was 53.2MW. Therefore, it should be noted that, these results verify that the proposed BESS sizing optimization approach minimizes the BESS capacity and total cost.

B. 14-BUS SYSTEM

The 14-bus system contains 20 transmission lines and 5 power generation units. Additionally, there are 5 PV generators and 5 BESSs. In this system, 259.3 MW is equally distributed among the five loads. Table 3 depicts six scenarios based on the PV capacity and maximum error in the 14-bus system. The scenarios are classified into three types, namely I, II, and III, according to the PV capacities of 50, 100, and 200 MW, respectively. Scenarios I-2, II-2, and III-2 increase the maximum PV forecast error by 50% compared to those of Scenarios I-1, II-1, and III-1, indicating whether the forecast variability is adequate in each case following the combined PC and BESS operation system. These scenarios

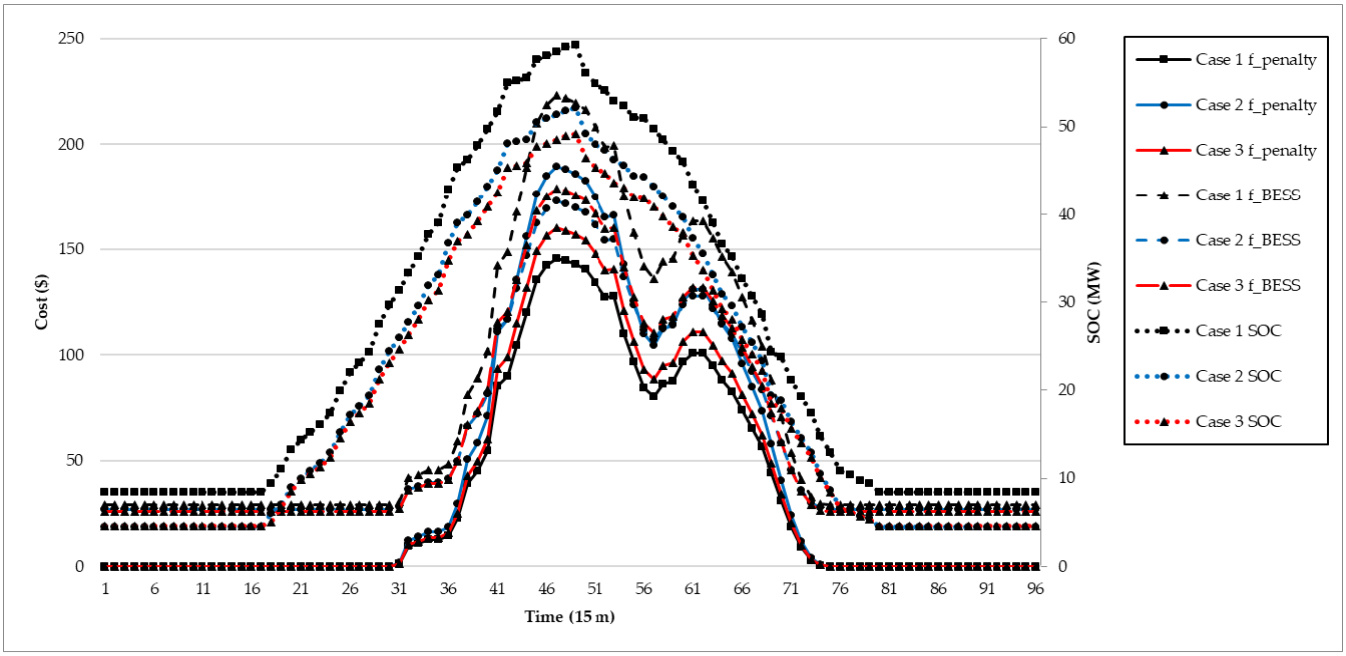

FIGURE 8. Confidence rate cost and SOC of each case.

TABLE 3. Scenario classification for PV capacity and maximum error.

Scenario	PV_P (MW)	e_{max} (p.u.)
I-1	50	1
I-2	50	1.5
II-1	100	1
II-2	100	1.5
III-1	200	1
III-2	200	1.5

represent the response of large disturbances caused by unexpected irradiation beyond the PV input data.

Table 4 presents the optimal results according to the scenarios. In all scenarios for Case 1, the PV capacity increases, and then the BESS and penalty cost increase at a similar rate. However, the power generation cost decreases as the PV capacity increases. The total cost decreases by approximately $130,000 in Scenario III-1 compared to that in Scenario I-1, and a BESS capacity of 374 MW is obtained for a PV generator capacity of 200 MW. In Scenarios I-2, II-2, and III-2, the BESS size does not change even though the maximum error increases. In Case 1, the BESS capacity was set to change according to the PV size. However, when the error increases to 50%, the penalty cost increases by approximately $300,000.

As shown in Scenarios I, II, and III of Case 2, the capacity of the battery slightly increases compared to that in Case 1. Owing to the characteristics of Case 2, which does not consider security constraints, the penalty cost is slightly increased in Scenarios I-1, II-1, and III-1 compared to that in Case 1. However, it is significantly lower than that in Case 1, while reflecting PV errors.

In Case 3, the penalty cost was as low as $326,000 and the BESS cost was as low as $250,000, and the overall scenario showed significant cost savings compared to other cases. In addition, when the prediction error increases, the BESS capacity of 423 MW, which is 82 MW less than that of Case 2, reduces penalty costs and power generation costs by approximately $246,000. Based on these results, Case 3 exhibits the most suitable result compared to those of other cases, despite the increase in PV capacity and prediction error. Therefore, these results confirm that the proposed approach exhibits the most promising results for any PV capacity and unexpected PV variability.

To demonstrate the superiority of D-PSCOPF, performance tests were conducted while comparing with other optimizations. Comparative optimizations are considered, such as OPF, SCOPF, and PSCOPF in Scenario III-2 of Case 3. SCOPF and PSCOPF are the addition of the several constraints to the conventional OPF. Table 5 shows the performance results for each methodology, including total cost, penalty cost and CPU time. All methods resulted in very high penalty cost in Case 1, and the resulting total cost was also the highest in Case 1. OPF, in which it is difficult to reflect the uncertainty of PV generation, had the highest penalty cost and total cost in all cases compared to other methods. Meanwhile, D-PSCOPF shows the lowest cost in all cases compared to PSCOPF, which reflects the probabilistic output of PV. In case 1 of OPF, the calculation was completed in the shortest time due to the simple optimization configuration compared to other methods. However, as the case became

TABLE 4. Optimal results for each scenario on Case 1, 2 and 3.

Case	Scenario	Penalty Cost ($)	BESS Cost ($)	Generation Cost ($)	Total Cost ($)	BESS Capacity (MW)
1	I-1	4,543	11,973	1,407,570	1,424,087	100
	I-2	19,080	11,973	1,407,570	1,438,624	100
	II-1	8,768	2,3107	1,309,040	1,340,916	193
	II-2	94,448	23,107	1,309,040	1,426,597	193
	III-1	17,009	44,829	1,230,498	1,292,337	374
	III-2	353,355	44,829	1,230,498	1,628,682	374
2	I-1	5,851	9,656	1,392,977	1,408,456	93.3
	I-2	6,436	74,953	1,434,766	1,516,156	139
	II-1	11,584	19,118	1,295,469	1,326,172	188
	II-2	12,743	148,408	1,334,333	1,495,484	248
	III-1	22,243	37,855	1,165,922	1,226,020	352
	III-2	24,467	293,848	1,200,899	1,519,215	505
3	I-1	5,045	10,083	1,366,458	1,381,587	88.7
	I-2	7,617	15,426	1,352,793	1,375,838	122
	II-1	9,333	18,653	1,202,483	1,230,470	164
	II-2	14,093	26,997	1,210,458	1,251,549	227
	III-1	16,613	33,576	1,058,185	1,108,375	306
	III-2	26,495	44,545	1,073,794	1,144,835	423

TABLE 5. Comparison results.

Method	Case	Total Cost ($)	Penalty Cost ($)	CPU Time (s)
OPF	1	1,930,131	451,003	9.81
	2	1,709,411	39,780	28.40
	3	1,215,350	33,843	78.55
SCOPF	1	1,785,820	380,989	13.32
	2	1,601,232	33,511	39.63
	3	1,201,132	34,213	146.52
PSCOPF	1	1,687,120	375,801	13.71
	2	1,532,155	32,121	41.59
	3	1,196,972	31,945	155.26
D-PSCOPF	1	1,628,682	353,355	9.88
	2	1,519,215	24,467	11.55
	3	1,144,835	26,495	14.12

more complex, the CPU time of Case 3 increased by 8 times compared to Case 1 to record 78.55 seconds. The CPU time of SCOPF and PSCOPF in all cases are almost similar because PSCOPF is almost the same as SCOPF with some added constraints. In case of adopting the conventional operation method of BESS as in Case 1, the CPU time difference between the existing SCOPF and D-PSCOPF is only approximately 4 s. However, in Case 2, wherein the BESS capacity is flexibly changed, the computation speed of SCOPF increases by approximately three times. Furthermore, Case 3, which considers the BESS sizing and security constraints, demonstrates an exponential increase of more than 11 times that in Case 1. Using the master-slave problem decomposition, Cases 2 and 3 of D-PSCOPF demonstrate a linear trend for the increase in computation time. In addition, D-PSCOPF requires approximately 18% of the computation time of OPF, which is a simple optimization, in Case 3. Therefore, these results reveal that the proposed D-PSCOPF is accurate and efficient for solving BESS sizing optimization for use with PV generation. As the system becomes larger, it becomes difficult to represent the entire process by a simple system equation, the calculation time increases, and the convergence of a specific search area is not guaranteed; the direct optimization of process simulation is limited in scope.

VII. CONCLUSION

In this study, a new computationally efficient optimization method, D-PSCOPF, was developed and used to perform BESS sizing optimizations in MGs, considering the stochastic fluctuation of PV outputs. This method enables a flexible preparation for the volatility of PV while sizing the capacity of BESS to a reasonable scale. To track the planned output of the PV, the optimized BESS was used to compensate

the prediction error. A PV fluctuation smoothing strategy based on dynamic SOC regulation was addressed in the MG. Our strategy increased the accuracy of the combined PV-BESS operation system through the BESS compensation strategy reflecting the rated output/capacity and life degradation model of the BESS. To optimize the BESS sizing under the constraint of a certain compensation degree, the compensation interval of the forecasting error should be first obtained in the combined PV-BESS. Our study determined the optimal interval, and then obtained the partial optimal BESS sizing to minimize the cost from the installation of the PV-BESS. This partial optimal BESS capacity was added as a BESS constraint to the D-PSCOPF problem, and the penalty cost of PV was then derived using the BESS capacity. According to the D-PSCOPF, this problem can be effectively solved by dividing it into a master problem and slave problem. In the slave problem, the base case solution was calculated. Using this value, the PV penalty cost was obtained, and this cost was again included in the constraints of the slave problem, which includes the BESS sizing process. When a violation occurs, a feasibility cut is added to the master problem. If there is no violation, the optimal BESS size can be derived. The superiority of the proposed BESS sizing optimization is proved through simulations with other cases under the condition of maintaining system stability. The proposed BESS size optimization approach derives the most reasonable BESS capacity to handle PV variability compared to conventional PV-BESS operation methods. In addition, it yields stable and economical operation results in case of high penetration rate of PV or unexpected large disturbance. Moreover, the convenience of calculation and optimality of the results was demonstrated through comparison with other optimization methods. Our future work will proceed with BESS sizing optimization on larger-scale systems such as real power systems and shall explore more accurate and faster calculations of D-PSCOPF suitable for such larger systems.

REFERENCES

[1] H.-S. Ryu and M.-K. Kim, "Two-stage optimal microgrid operation with a risk-based hybrid demand response program considering uncertainty," *Energies*, vol. 13, no. 22, p. 6052, Nov. 2020.

[2] H. Yu and W. D. Rosehart, "An optimal power flow algorithm to achieve robust operation considering load and renewable generation uncertainties," *IEEE Trans. Power Syst.*, vol. 27, no. 4, pp. 1808–1817, Nov. 2012.

[3] A. Monticelli, M. V. F. Pereira, and S. Granville, "Security-constrained optimal power flow with post-contingency corrective rescheduling," *IEEE Trans. Power Syst.*, vol. PS-2, no. 1, pp. 175–180, Feb. 1987.

[4] M. K. Kim, D. Hur, and J. Park, "Determination of available transfer capability using multi-objective contingency constrained optimal power flow with post-contingency corrective rescheduling," *Electr. Eng.*, vol. 90, no. 4, pp. 243–253, Apr. 2008.

[5] Y. T. Tan, D. S. Kirschen, and N. Jenkins, "A model of PV generation suitable for stability analysis," *IEEE Trans. Energy Convers.*, vol. 19, no. 4, pp. 748–755, Dec. 2004.

[6] H. A. M. Maghraby, M. H. Shwehdi, and G. K. Al-Bassam, "Probabilistic assessment of photovoltaic (PV) generation systems," *IEEE Trans. Power Syst.*, vol. 17, no. 1, pp. 205–208, Jan. 2002.

[7] T. Beck, H. Kondziella, G. Huard, and T. Bruckner, "Assessing the influence of the temporal resolution of electrical load and PV generation profiles on self-consumption and sizing of PV-battery systems," *Appl. Energy*, vol. 173, pp. 331–342, Jul. 2016.

[8] A. Ellis, D. Schoenwald, J. Hawkins, S. Willard, and B. Arellano, "PV output smoothing with energy storage," in *Proc. 38th IEEE Photovolt. Spec. Conf.*, Jun. 2012, pp. 1523–1528.

[9] R. K. Lam and H.-G. Yeh, "PV ramp limiting controls with adaptive smoothing filter through a battery energy storage system," in *Proc. IEEE Green Energy Syst. Conf. (IGESC)*, Nov. 2014, pp. 55–60.

[10] X. Li, D. Hui, and X. Lai, "Battery energy storage station (BESS)-based smoothing control of photovoltaic (PV) and wind power generation fluctuations," *IEEE Trans. Sustain. Energy*, vol. 4, no. 2, pp. 464–473, Apr. 2013.

[11] W. Kreeumpornand and I. Ngamroo, "Optimal superconducting coil integrated into PV generators for smoothing power and regulating voltage in distribution system with PHEVs," *IEEE Trans. Appl. Supercond.* vol. 26, no. 7, Oct. 2016, Art. no. 5402805.

[12] A. Awad, I. Tumar, M. Hussein, W. Ghanem, and J. A. Sa'ed, "PV output power smoothing using flywheel storage system," in *Proc. IEEE Int. Conf. Environ. Electr. Eng.*, Jun. 2017, pp. 1–6.

[13] C. Bharatiraja, S. Jeevananthan, and R. Latha, "FPGA based practical implementation of NPC-MLI with SVPWM for an autonomous operation PV system with capacitor balancing," *Int. J. Electr. Power Energy Syst.*, vol. 61, pp. 489–509, Oct. 2014.

[14] B. Vatandoust, A. Ahmadian, M. A. Golkar, A. Elkamel, A. Almansoori, and M. Ghaljehei, "Risk-averse optimal bidding of electric vehicles and energy storage aggregator in day-ahead frequency regulation market," *IEEE Trans. Power Syst.*, vol. 34, no. 3, pp. 2036–2047, May 2019.

[15] H. Ren, Q. Wu, W. Gao, and W. Zhou, "Optimal operation of a grid-connected hybrid PV/fuel cell/battery energy system for residential applications," *Energy*, vol. 113, pp. 702–712, Oct. 2016.

[16] W. Ko and M.-K. Kim, "Operation strategy for maximizing revenue of an energy storage system with a photovoltaic power plant considering the incentive for forecast accuracy in South Korea," *IEEE Access*, vol. 9, pp. 71184–71193, 2021.

[17] Y. Yang, H. Li, A. Aichhorn, J. Zheng, and M. Greenleaf, "Sizing strategy of distributed battery storage system with high penetration of photovoltaic for voltage regulation and peak load shaving," *IEEE Trans. Smart Grid*, vol. 5, no. 2, pp. 982–991, Mar. 2013.

[18] M. Ahmed and S. Kamalasadan, "Energy storage PV capacity firming with forecasted power reference and optimal error minimization," in *Proc. North Amer. Power Symp. (NAPS)*, Oct. 2015, pp. 1–6.

[19] Y. Huang, P. Li, W. Wang, and L. Dong, "Capacity optimization of battery energy storage system in multi-energy complementary system based on time series simulation method," in *Proc. Innov. Smart Grid Technol.-Asia (ISGT Asia)*, May 2019, pp. 3804–3809.

[20] H. Le and T. Nguyen, "Sizing energy storage systems for wind power firming: An analytical approach and a cost-benefit analysis," in *Proc. IEEE Power Energy Soc. Gen. Meeting-Convers. Del. Elect. Energy*, Jul. 2008, pp. 1–8.

[21] R. Atia and N. Yamada, "Sizing and analysis of renewable energy and battery systems in residential microgrids," *IEEE Trans. Smart Grid*, vol. 7, no. 3, pp. 1204–1213, May 2016.

[22] B.-R. Ke, T.-T. Ku, Y.-L. Ke, C.-Y. Chuang, and H.-Z. Chen, "Sizing the battery energy storage system on a university campus with prediction of load and photovoltaic generation," *IEEE Trans. Ind. Appl.*, vol. 52, no. 2, pp. 1136–1147, Apr. 2016.

[23] J. Dulout, B. Jammes, C. Alonso, A. Anvari-Moghaddam, A. Luna, and J. M. Guerrero, "Optimal sizing of a lithium battery energy storage system for grid-connected photovoltaic systems," in *Proc. IEEE 2nd Int. Conf. DC Microgrids (ICDCM)*, Jun. 2017, pp. 582–587.

[24] C. Nayak and M. Nayak, "Optimal battery energy storage sizing for grid connected PV system using IHSA," in *Proc. Int. Conf. Signal Process., Commun., Power Embedded Syst. (SCOPES)*, Oct. 2016, pp. 121–127.

[25] X. Zhu, J. Yan, and N. Lu, "A graphical performance-based energy storage capacity sizing method for high solar penetration residential feeders," *IEEE Trans. Smart Grid*, vol. 8, no. 1, pp. 3–12, Jan. 2017.

[26] N. Rezaei, A. Ahmadi, A. Khazali, and J. Aghaei, "Multiobjective risk-constrained optimal bidding strategy of smart microgrids: An IGDT-based normal boundary intersection approach," *IEEE Trans. Ind. Informat.*, vol. 15, no. 3, pp. 1532–1543, Mar. 2019, doi: 10.1109/TII.2018.2850533.

[27] M. K. Kim and D. Hur, "An optimal pricing scheme in electricity markets by parallelizing security constrained optimal power flow based market-clearing model," *Int. J. Electr. Power Energy Syst.*, vol. 48, pp. 161–171, Jun. 2013.

[28] J.-K. Lyu, M.-K. Kim, and J.-K. Park, "Security cost analysis with linear ramp model using contingency constrained optimal power flow," *J. Electr. Eng. Technol.*, vol. 4, no. 3, pp. 353–359, Sep. 2009.

[29] P. P. Gupta, P. Jain, S. Sharma, and R. Bhaker, "Security constrained unit commitment in a power system based on battery energy storage with high wind penetration," in *Proc. Int. Conf. Power, Instrum., Control Comput. (PICC)*, Jan. 2018, pp. 1–6.
[30] J. Sa'ed, S. Favuzza, F. Massaro, and E. Telaretti, "Optimization of BESS capacity under a peak load shaving strategy," in *Proc. IEEE Int. Conf. Environ. Electr. Eng.*, Jun. 2018, pp. 1–4.
[31] S. Chen, T. Zhang, H. B. Gooi, R. D. Masiello, and W. Katzenstein, "Penetration rate and effectiveness studies of aggregated BESS for frequency regulation," *IEEE Trans. Smart Grid*, vol. 7, no. 1, pp. 167–177, Jan. 2016.
[32] L. Zhou, Y. Zhang, X. Lin, C. Li, Z. Cai, and P. Yang, "Optimal sizing of PV and BESS for a smart household considering different price mechanisms," *IEEE Access*, vol. 6, pp. 41050–41059, 2018.
[33] Y.-R. Lee, H.-J. Kim, and M.-K. Kim, "Optimal operation scheduling considering cycle aging of battery energy storage systems on stochastic unit commitments in microgrids," *Energies*, vol. 14, no. 2, p. 470, Jan. 2021.
[34] W.-W. Kim, J.-S. Shin, S.-Y. Kim, and J.-O. Kim, "Operation scheduling for an energy storage system considering reliability and aging," *Energy*, vol. 141, pp. 389–397, Dec. 2017.
[35] A. M. Geoffrion, "Generalized benders decomposition," *J. Optim. Theory Appl.*, vol. 10, no. 4, pp. 237–260, Oct. 1972.
[36] A. Khodaei, "Microgrid optimal scheduling with multi-period islanding constraints," *IEEE Trans. Power Syst.*, vol. 29, no. 3, pp. 1383–1392, May 2014.
[37] B. Liu, F. Liu, B. Zhai, and H. Lan, "Investigating continuous power flow solutions of IEEE 14-bus system," *IEEJ Trans. Electr. Electron. Eng.*, vol. 14, no. 1, pp. 157–159, Jan. 2019.
[38] Elia Group. (2021). *Solar Power Generation*. [Online]. Available: https://www.elia.be/en/grid-data/power-generation/solar-pv-power-generation-data

YONG-RAE LEE received the B.S. and M.S. degrees from the School of Energy System Engineering, Chung-Ang University, Seoul, South Korea, in 2018 and 2021, respectively. His research interests include power system operation, renewable energy resources, microgrids, and BESS utilization.

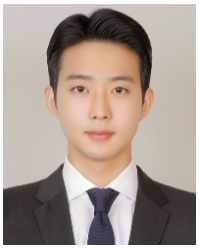

HYUN-JOON KANG received the B.S. degree from the School of Energy System Engineering, Chung-Ang University, Seoul, South Korea, in 2021, where he is currently pursuing the M.S. degree. His research interests include electric vehicles and vehicle-to-grid.

MUN-KYEOM KIM received the Ph.D. degree in electrical and computer engineering from Seoul National University. He is currently a Professor with the School of Energy System Engineering, Chung-Ang University, Seoul, South Korea. His research interests include operational techniques in hybrid ac/dc power systems, AI-based smart power networks, big data-based demand response, real-time market design, and multi-agent-based smart city intelligence.